Adaptive Frequency Sampling Based on Local Rational Modeling for Microwave Electromagnetic Simulations

Dries Peumans, *Member, IEEE*, Sander De Keersmaeker, *Student Member, IEEE*, Cedric Busschots, *Member, IEEE*, Yves Rolain, *Fellow, IEEE*, and Francesco Ferranti, *Senior Member, IEEE*

***Abstract*— Performing simulations with electromagnetic (EM) solvers can be a computationally complex task that is time consuming and resource demanding. Adaptive frequency sampling (AFS) techniques are very effective in reducing the computational complexity of frequency-domain simulations performed by EM solvers. In this work, we propose a novel AFS technique based on local rational models. This brings multiple advantages, such as accurate and efficient model uncertainty estimation, the local refinement of subintervals of the full frequency range of interest, and suitability toward parallel computing. Multiple numerical examples thoroughly validate the proposed technique. The local rational models can also be used as an accurate frequency-domain macromodeling technique after the AFS process is completed.**

***Index Terms*— Adaptive sampling, frequency-domain modeling, frequency-domain simulations, local rational modeling.**

I. Introduction

ELECTROMAGNETIC (EM) simulation tools are necessary tools for the design of a variety of systems, such as microwave filters, antennas, high-speed interconnects, and printed circuit boards. The frequency-domain behavior of these systems can result quite complex (e.g., multiple resonances and antiresonances). Performing EM computations with an EM solver (e.g., the method of moments, finite-element method, and partial eElement equivalent circuit (PEEC) methods [1], [2], [3], [4]) can be a computationally complex task that is time consuming and resource demanding. Therefore, one very often needs to restrict the number of computed frequency samples in order to obtain results in an acceptable time frame. Consequently, valuable system characteristics, such as (anti-)resonances and coupling effects, can be partly identified or even missed.

Adaptive frequency sampling (AFS) algorithms are often used to find a minimal set of frequencies, in such a way that each frequency sample contains as much valuable information as possible about the system's behavior. In the literature, adaptive sampling is also sometimes denoted by active learning. Current AFS algorithms add additional frequency data samples in an iterative way without requiring any prior system knowledge [5], [6], [7], [8], [9], [10]. In each consecutive iteration, a data-driven model order reduction (MOR) method is used to steer the frequency sampling process. The aim of these MOR methods is to capture the frequency-dependent behavior of microwave systems with a reduced-order macromodel [11], [12], [13], [14]. In the microwave community, vector fitting (VF) is a very widely adopted data-driven MOR technique [12], [13], [15]. Starting from data available at a discrete set of frequencies, VF uses rational least-squares estimation to produce a reduced frequency-domain macromodel. VF has become popular mainly due to its numerical robustness in estimating high-order models, and the ease of physical interpretation with the adoption of the pole-residue format. Depending on the AFS algorithm used, one or multiple frequency-domain macromodels with varying model order need to be identified to quantify the model uncertainty. The model uncertainty is used here as a metric to determine in which frequency regions the response of the system should be sampled more densely. Therefore, the AFS algorithm adds additional frequency data samples in those frequency regions, where the uncertainty exceeds a certain threshold level. The proper functioning of existing AFS algorithm depends greatly on the assumption that the response of the system can be approximated sufficiently well by a global macromodel. As the name suggests, a global macromodel aims to capture the dynamic response of a system over the whole frequency band of interest. This has the advantage that only one single, potentially complicated, model is needed. The downside of using a global model is that generally extensive model order selection is required to eliminate both overfitting and undermodeling.

Another important aspect to consider is that the distributed character of a microwave system introduces a propagation delay. For a transfer function type of format (i.e., S-, Z-,

Manuscript received 15 December 2023; accepted 12 January 2024. Date of publication 30 January 2024; date of current version 7 August 2024. This work was supported in part by the Strategic Research Program of Vrije Universiteit Brussel (SRP-19 and SRP-78), in part by the Methusalem and Hercules Foundations, and in part by the Research Council (OZR) of the Vrije Universiteit Brussel. *(Corresponding author: Dries Peumans.)*

Dries Peumans, Sander De Keersmaeker, and Yves Rolain are with the Department of Fundamental Electricity and Instrumentation, Vrije Universiteit Brussel, 1050 Brussels, Belgium (e-mail: dries.peumans@vub.be).

Cedric Busschots is with the Royal Belgian Institute for Space Aeronomy, 1180 Brussels, Belgium.

Francesco Ferranti is with the Department of Applied Physics and Photonics, Brussels Photonics, Vrije Universiteit Brussel, 1050 Brussels, Belgium, and also with Flanders Make, 1050 Brussels, Belgium.

Color versions of one or more figures in this article are available at https://doi.org/10.1109/TMTT.2024.3355270.

Digital Object Identifier 10.1109/TMTT.2024.3355270

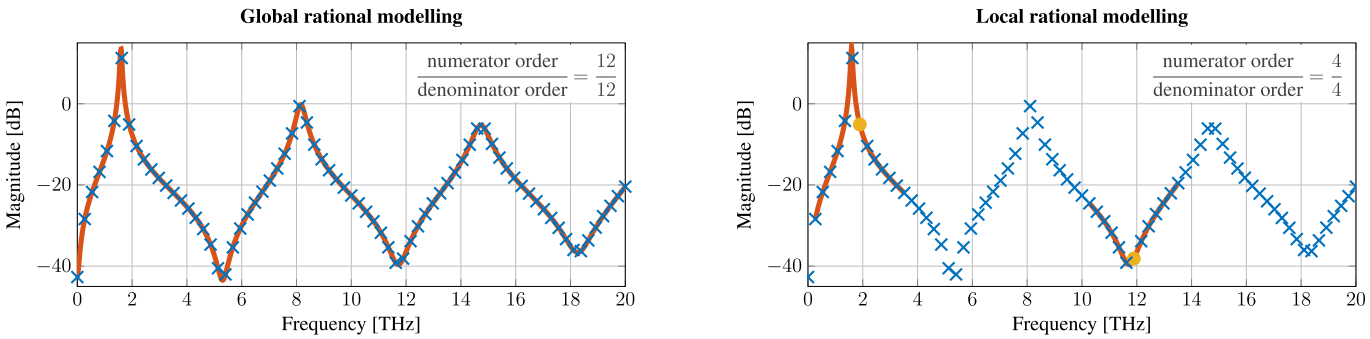

Fig. 1. Global rational modeling focuses on the whole frequency band of interest. Local rational modeling only uses on a sub-band around a specific center frequency. ×: available data, −: estimated rational model, and •: center frequency.

or Y-parameters) this delay expresses itself through terms in an exponential form $e^{-s\tau}$ in the frequency domain, where s denotes the complex Laplace variable and τ denotes a delay term. As a result, global rational models generally endure a significant increase in model order complexity merely for the sake of fitting the complex exponential terms.

In recent years, local rational modeling (LRM) techniques have been introduced that greatly mitigate the computational complexity associated with model order selection [16], [17]. The advantages of these local techniques have already been demonstrated in the context of AFS [18], [19]. By only focusing on a small sub-band around a specific center frequency, the local dynamic variations can more be easily modeled by a low-order rational approximation model. This is an attractive feature for microwave systems that often contain the influence of time delays in their dynamic behavior. The basic idea behind any LRM techniques is to approximate the dynamic behavior of a system with a local rational model as a function of the frequency f. Fig. 1 illustrates the major difference between global and local rational models.

In this article, we propose a novel AFS technique based on local rational models. There are several main advantages of using local rational models, which provide a very valuable and solid foundation for advanced AFS techniques. Below, we summarize these advantages.

1) The use of accurate and efficient uncertainty estimation metrics without the need for a model order selection to drive the convergence of the AFS method. AFS techniques based on global models might likely need to refine the model order as needed, while the sampling iterations advance.
2) The estimation of local rational models does not necessarily need to be repeated at all frequencies in each iteration. Once all the rational models are obtained after the first iteration, consecutive iterations only need to update the models around those frequencies that are affected by the inclusion of new frequency samples.
3) Local rational models can better handle the distributed behavior of microwave systems with respect to global rational models.
4) Furthermore, local rational modeling is very suitable for using in parallel computing.

We highlight that the use of local rational models in this work is focused on the development of a novel AFS approach. After the AFS is carried out, any modeling techniques suitable for frequency-domain data samples (as the VF approach) can be used based on the collected data. It is important to note that the local rational models can also be used as an accurate frequency-domain macromodeling technique after the AFS process is completed. The proposed technique can be very useful in multiple simulation and modeling tasks such as fast frequency-sweeping for EM simulations and the significant reduction of the CPU time needed to collect the EM data samples for parameterized modeling techniques [20], [21], [22], [23], where multiple EM simulations as a function of design parameters have to be carried out.

This article is organized as follows. Section II introduces existing AFS techniques and provides a review of the current state of the art. Section III discusses the fundamental concepts of LRM techniques. Section IV describes the proposed AFS algorithm. Section V shows the extensive numerical results that validate the accuracy and efficiency of the proposed AFS method. The conclusion is drawn in Section VI.

II. Existing AFS Techniques

Over the years, numerous AFS algorithms have been developed, using global rational macromodeling techniques [5], [6], [7], [8], [9], [10]. These algorithms employ a global rational macromodel, represented by a partial fraction expansion

$$R(f) = \sum_{i=1}^{n_p} \frac{c_i}{j2\pi f - p_i} + d. \tag{1}$$

Here, c_i represents the residues associated with the poles p_i, and d is a real constant. Irrespective of the estimation technique employed to determine the unknown coefficients in the expansion, current AFS techniques use these rational models to automatically select the next sampling frequency location.

In general, current AFS algorithms follow a two-step approach. In the first step, multiple rational models with varying orders (n_p) are fit using the available data samples. The model order is initially set to a low value and iteratively increased until the model error falls below a predefined accuracy threshold. This step aims to improve the model accuracy by adjusting the complexity of the rational model. In the second step, the two models with the lowest model error are selected and compared using a set of rules known as reflective functions [7]. These reflective functions provide

a basis for evaluating the model quality and determining the next sampling location. Based on the outcome of the reflective functions, the algorithm selects the next sampling location and the entire two-step procedure is reinitialized. This iterative process allows for refining the sampling strategy and improving the accuracy of the models as more information is gathered.

Although AFS techniques have demonstrated high efficiency, they depend on an important assumption that the data samples can be accurately approximated by the estimated global rational models. However, a challenge arises when the dynamic behavior of the system is such that even with large model orders, the global rational model yields a substantial model error. In such cases, comparing the "best" rational models would lead to an erroneous comparison, and consequently, the selection of the next frequency sample would be incorrect. This limitation highlights the need for an alternative approach that can handle situations where a global model fails to accurately represent the system's behavior. To address this limitation, we have incorporated local rational modeling techniques, which offer two significant advancements. First, we employ an error assessment that directly measures the discrepancy between the model and the data samples. This approach eliminates the reliance on reflective functions that compare models against each other. By focusing on the direct error evaluation, we can more accurately assess the adequacy of the model and avoid erroneous comparisons. Second, the integration of local rational modeling techniques allows us to eliminate the need for model order selection. This reduction in computational load simplifies the AFS algorithm and improves its efficiency.

III. Local Rational Modeling Techniques

This section provides the necessary background for the proposed AFS algorithm. It discusses the fundamental concepts underlying the proposed LRM technique.

In this article, we use the matrix $\boldsymbol{X}(f) \in \mathbb{C}^{N\times N}$ to describe the electrical input–output behavior of an N-port system as a function of the frequency f. $\boldsymbol{X}$ can denote multiple representations of interest, such as the impedance, admittance, and scattering parameters. We assume that simulation/measurement data of $\boldsymbol{X}$ is available at a set of frequencies $\xi = \{f_1, \ldots, f_k, \ldots, f_F\}$ $(k = 1, \ldots, F)$. In general, the local modeling technique does not assume reciprocity for the N-port system being analyzed. However, if the matrix $\boldsymbol{X}$ is, indeed, reciprocal, then, it is only necessary to consider either the upper or lower triangular portion of $\boldsymbol{X}$ for modeling and analysis purposes.

The underlying concept of these local modeling techniques is to approximate the behavior of $\boldsymbol{X}$ at each frequency f_k with a local rational model. As $\boldsymbol{X}$ is expected to be a smooth function of f_k, practically any continuous function can be employed for this purpose. Among the popular choices, polynomial matrices [24] and rational matrix parameterizations [17] have exhibited remarkable outcomes in the past. To illustrate the functioning of these local modeling techniques, let us assume that we aim to estimate $\boldsymbol{X}(f_k)$ through a local rational model. For this estimation, a local set of frequencies f_{k+r} centered around f_k is used to approximate $\boldsymbol{X} \in \mathbb{C}^{N\times N}$ with a common-denominator rational model

$$\boldsymbol{X}(f_{k+r}) = \boldsymbol{X}(f_k + \delta_r) \approx \frac{\boldsymbol{B}_k(\delta_r)}{A_k(\delta_r)} \tag{2}$$

where $r \in \{-n_f, \ldots, -1, 0, 1, \ldots, n_f\}$. δ_r quantifies the local frequency variation around the center frequency f_k. The total number of data points considered for the estimation in the local sub-band equals $2n_f + 1$. The complex numerator and denominator matrix polynomials $\boldsymbol{B}_k$ and A_k are defined as follows:

$$\boldsymbol{B}_k(\delta_r) = \sum_{n=0}^{n_B} \boldsymbol{b}_{kn}\, \delta_r^n \quad A_k(\delta_r) = \sum_{n=0}^{n_A} a_{kn}\, \delta_r^n \tag{3}$$

where $\boldsymbol{b}_{kn} \in \mathbb{C}^{N\times N}$ and $a_{kn} \in \mathbb{C}$ are the unknown rational model coefficients that capture the dynamic variations within each local model. n_B and n_A define the model order of the denominator and numerator polynomial, respectively.

Over recent years, several estimation techniques with varying computational complexity have been proposed to identify the coefficients of the local rational model (see [17], for an overview). The goal of any of these techniques is to solve the following least-squares minimization problem:

$$\min_{\boldsymbol{\theta}_k} \sum_{r=-n_f}^{n_f} \left\| \boldsymbol{X}(f_k + \delta_r) - \frac{\boldsymbol{B}_k(\delta_r)}{A_k(\delta_r)} \right\|_2^2 \tag{4}$$

where $\boldsymbol{\theta}_k$ is the stacked vector of all unknown model coefficients $\boldsymbol{b}_{kn}$ and a_{kn}. Since (4) contains a division by the denominator polynomial, the minimization problem becomes inherently nonlinear in the parameters. Finding an optimal solution to (4), therefore, generally requires an iterative minimization scheme (Gauss–Newton and Levenberg–Marquardt) that is computationally expensive. To lower the computational complexity, it is common practice to linearize the original problem in (4) by multiplication with the denominator polynomial $A_c(\delta_r)$ (e.g., Levy, Sanathanan–Koerner, and vector fitting). The cost of performing this linearization is that a bias is introduced during the estimation [16]. To counteract this linearization bias, we choose to use the so-called bootstrapped total-least squares (BTLSs) estimator [25]. The BTLS estimator is an iterative total-least squares estimator that provides an unbiased estimate of the local model coefficients, even when $\boldsymbol{X}$ is corrupted with noise.

The estimation of the local rational model is influenced by three hyperparameters that regulate the estimation process. These hyperparameters are the model orders, n_B and n_A, and the number of data points considered, $2n_f + 1$. Frequently, the last hyperparameter is substituted with the "degrees of freedom" (q) of the estimation. It is calculated by subtracting the total number of model parameters from the total number of local data points [17]

$$q = 2\, n_f + 1 - \frac{n_\theta}{N} \tag{5}$$

with

$$n_\theta = n_A + (n_B + 1)\, N^2. \tag{6}$$

An essential aspect of local modeling techniques is determining optimal values for the hyperparameters. As the model order increases, it enhances not only the modeling capability but it also inevitably widens the sub-bands width for a constant number of degrees of freedom [see (5)]. This widening leads to more dynamic variations that the model needs to capture. Consequently, boosting the model orders does not always result in better modeling accuracy. After extensive application of the local modeling methods in diverse application areas, encompassing both mechanical and EM domains, it has been observed that utilizing polynomial orders up to the 8th degree in conjunction with 6 or 8 degrees of freedom typically strikes a beneficial balance between model complexity and sub-band width [16], [17].

Since optimization is executed in a least-squares sense, the residuals (which represent the disparity between the original data and the estimated model) encapsulate the combined impact of two types of uncertainty.

1) *Model Uncertainty:* A poor model selection results in overfitting or underfitting of the provided data.
2) *Noise Uncertainty:* Data samples can be corrupted by noise. Stochastic noise remains present in the residuals since the model only aims to capture the deterministic behavior of the system.

Depending on the type of uncertainty that is dominant, different metrics can be used to quantify the uncertainty. In a simulation setting, the model uncertainty is considered dominant as no measurement noise is present. Therefore, most often the (weighted) magnitude of the residual $\boldsymbol{\epsilon}_k$ is adopted as a metric

$$|\boldsymbol{\epsilon}_k(\delta_r)| = \left| \boldsymbol{X}(f_k + \delta_r) - \frac{\boldsymbol{B}_k(\delta_r)}{A_k(\delta_r)} \right|. \tag{7}$$

In a measurement setting, on the other hand, the noise uncertainty plays an important role and other metrics can be used. The scope of this article is on simulated data; therefore, we do not tackle the case of noisy data, which is future work.

The local rational modeling assumes that n_f frequencies are available at the left- and right-hand sides of each frequency f_k. This is not the case at the left and right borders of the frequency set $\{f_k\}$. At those borders, an asymmetric window is used to resolve this issue. The first and last n_f+1 frequencies of ξ use the same sub-band for the rational model estimation, which inevitably results in the same estimated local rational model. As a consequence, the estimated uncertainty is constant at the borders.

IV. Proposed Adaptive Sampling Algorithm

This section describes the proposed AFS algorithm that uses local rational macromodels to guide the sampling process in an iterative way. In each consecutive iteration, the proposed technique runs through some steps to make an optimal decision (see Fig. 2). A more in-depth explanation of each step is provided in the following paragraphs.

Step 0 (Initialization): To start the AFS algorithm, we need an initial set of samples $\boldsymbol{X}(f_k)$ that are simulated at evenly spaced intervals across the frequency range of interest $[f_{\min}, f_{\max}]$. It is important to avoid having too many initial samples, as this defeats the purpose of the AFS algorithm. However, the minimum number of initial samples is equal to the sub-band width $2n_f + 1$. This width is determined by the degrees of freedom q and the model orders n_A and n_B in (5). It is recommended to add a margin to the minimum number of initial samples because if we use only the minimum number, we cannot shift the sub-band window, resulting in all local models using the same data. As a consequence, the uncertainty for each frequency f_k will be constant, making it impossible to make an initial decision with the AFS algorithm. For that reason, the total number of initial samples corresponds to the sub-band width derived from (5), augmented by half of the sub-band width n_f

$$F_{\min} = q + \left\lceil \frac{n_\theta}{N} \right\rceil + n_f \tag{8}$$

where $\lceil \bullet \rceil$ represents the ceil operator.

Step 1 (Estimation of Local Rational Models): The aim of Step 1 is to quantify the model uncertainty at each frequency f_k belonging to the current set $\xi = \{f_k\}(k = 1, \ldots, F)$. To do so, a local rational model first needs to be estimated at each frequency f_k using the LRM technique described in Section III. As mentioned earlier in Section III, the AFS algorithm's ability to select a minimal set of samples relies on the user's selection of the rational model hyperparameters (n_A, n_B, and q). To set these hyperparameters, the user can refer to some guidelines that are available. Section III already indicated that choosing polynomial orders up to the 8th degree, in combination with 6 or 8 degrees of freedom, strikes a balance between model complexity and sub-band width. In addition, it is advisable to set n_A equal to n_B, which ensures that the algorithm does not show any preference for modeling resonances or antiresonances. Earlier research has also demonstrated that selecting an even polynomial order can enhance the accuracy of the model in the (anti-)resonance regions [17]. Based on these two restrictions, there are only four possible options for the polynomial orders: $\{2, 4, 6, 8\}$. In general, the higher the polynomial orders chosen, the better the rational model's modeling capabilities for describing local dynamic variations (lower residual error), and the lower the number of samples that the AFS algorithm will need to select. It is worth noting that once the polynomial model orders n_A and n_B are selected, they remain fixed during the entire duration of the AFS algorithm. Consequently, the model uncertainty becomes a direct measure of the undersampling of $\boldsymbol{X}$.

Once the rational model estimation is finished, the model uncertainty is derived from the residuals $\boldsymbol{\epsilon}_k$ in (7). Many definitions exist to quantify the model uncertainty [26]. In a simulation-based scenario, a commonly used uncertainty metric μ is based on the computation of the maximum of the relative error across both the frequency δ_r and different input–output combinations

$$\mu(f_k) = \max_{\delta_r, i, j} \left\{ \left| \frac{\boldsymbol{\epsilon}_k^{[i,j]}(\delta_r)}{\boldsymbol{B}_k^{[i,j]}(\delta_r)/A_k(\delta_r)} \right| \right\} \tag{9}$$

where $\bullet^{[i,j]}$ selects the matrix element on the ith row and jth column. By defining uncertainty in this manner, we can

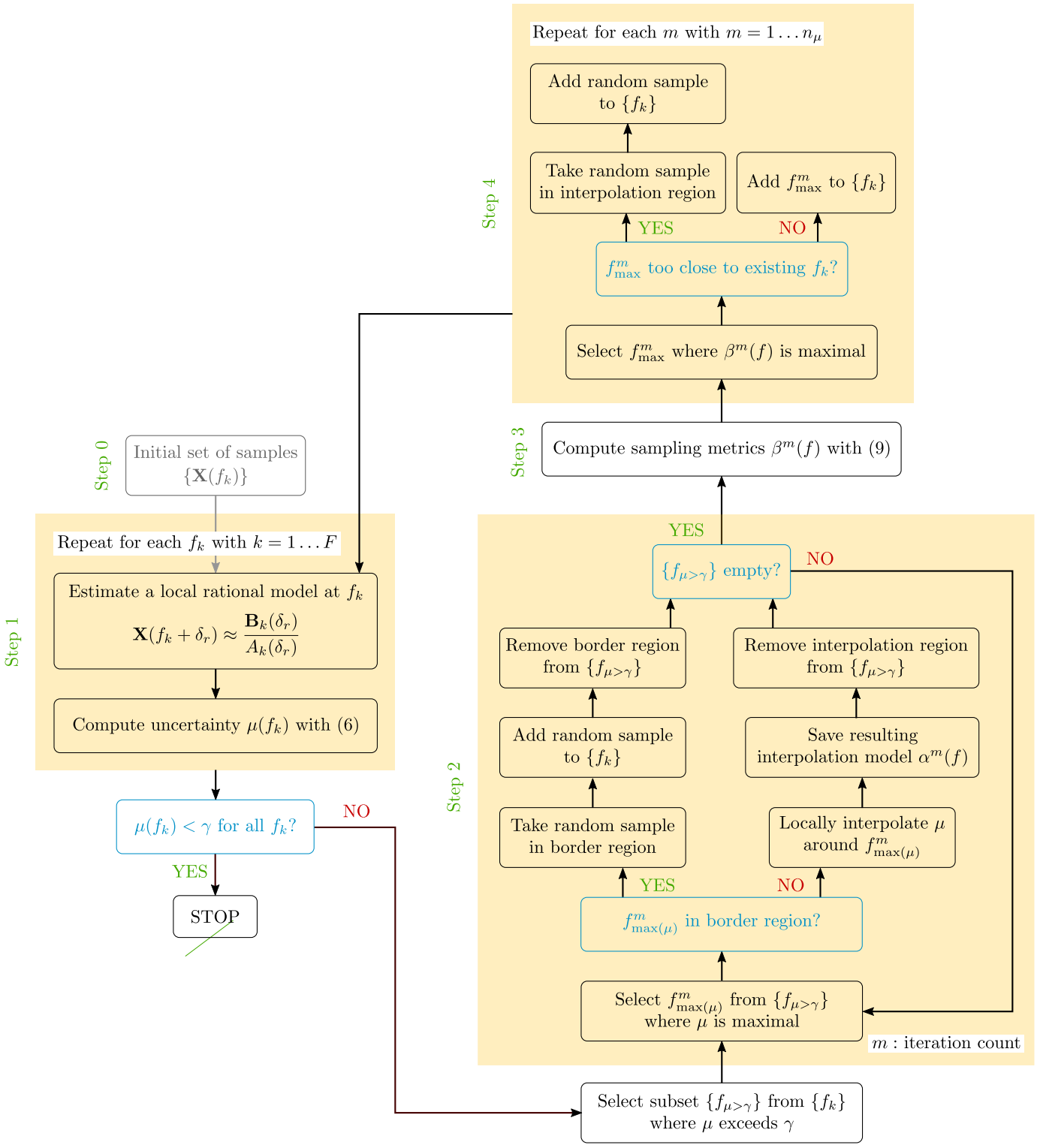

Fig. 2. Algorithmic overview of the proposed AFS technique. A thorough explanation of different steps is provided in Section IV.

ensure that the relative error remains bounded across all input–output combinations and frequencies, thereby providing a comprehensive evaluation of the model's accuracy on a global scale.

Local rational models not only provide an uncertainty metric but also serve as frequency-domain macromodels similar to global rational macromodels. Rather than relying on a single global model, we now have a rational model for each sample f_k, enabling local modeling in the vicinity of a given sample. For instance, if we need to predict the value of $\boldsymbol{X}$ at a specific frequency f, we can use the local rational model at the frequency f_k closest to f. Since a rational model is obtained for each sample f_k, a smooth prediction is achieved by overlapping sub-bands, which are shifted by

one frequency sample every time. Without these overlapping sub-bands, a discontinuous modeling behavior would occur at the boundaries.

Another advantage of the use of local rational models is that the estimation does not necessarily need to be reperformed at all frequencies during each iteration. Once all the rational models are obtained after the first iteration, consecutive iterations only need to update the models at those frequencies that are affected by the inclusion of new frequency samples. More specifically, only n_f frequencies to the left and the right of a novel sample require an update. Implementation of this updating scheme results in a highly efficient estimation. Furthermore, a high level of parallelism is possible as each local rational model is estimated independently.

Step 2 (Local Interpolation of the Model Uncertainty): After Step 1, an estimate of the uncertainty μ is available at the discrete set of frequencies $\{f_k\}$. If all these uncertainties are smaller than a user-defined accuracy level γ, the AFS algorithm can be stopped. If not, a model is required to assess the uncertainty in all the frequency regions where no samples are available. A straightforward way to obtain this model is by interpolation. However, many types of interpolation exist, each with their respective (dis)advantages [27]. We choose a local modeling flavor of the well-known cubic spline interpolation since it provides a good balance between computational complexity and attainable accuracy [28].

Global interpolation of the uncertainty with cubic splines does not yield accurate results. Due to the local rational modeling, the uncertainty shows a rapid decrease (almost discontinuous) in the frequency regions, where the dynamic deviations are modeled correctly. As a result, the cubic spline interpolation is afflicted by the Gibbs phenomenon [29]. The occurrence of the Gibbs phenomenon is prevented if the interpolation of μ is also performed in a local setting. To do so, an iterative scheme is devised that performs the local interpolation in an automatic way.

1) Set the iteration counter m equal to 1. Determine the set of frequencies $\{f_{\mu>\gamma}\} \subset \{f_k\}$, where μ exceeds the threshold level γ. The borders of $\{f_k\}$ (the $n_f + 1$ first and last frequencies) are excluded from this search as the uncertainty is constant in those regions. Instead, a random sample is taken in the border regions if the uncertainty exceeds the threshold level.
2) From $\{f_{\mu>\gamma}\}$, select the frequency $f^m_{\max(\mu)}$, where the uncertainty is maximal.
3) Locally interpolate μ with cubic splines in a sub-band around $f^m_{\max(\mu)}$. Similar to the local rational modeling in Step 1, the sub-band consists of a local set of frequencies $f^m_{\max(\mu)+r}$ from $\{f_{\mu>\gamma}\}$ where $r \in \{-n_f, \ldots, -1, 0, 1, \ldots, n_f\}$. If no n_f frequencies to the left or the right of $f^m_{\max(\mu)}$ are available in $\{f_{\mu>\gamma}\}$; then, the sub-band becomes asymmetric and only continues to the left or right boundary of $\{f_{\mu>\gamma}\}$. In the special case that $\{f_{\mu>\gamma}\}$ contains only a single point, use the n_f frequencies to the left and the right for the uncertainty interpolation. The resulting interpolation model of the model uncertainty is denoted by $\alpha^m(f)$. This interpolation model is only valid in the frequency interval $f \in [f^{\alpha^m}_{\min}, f^{\alpha^m}_{\max}]$. The boundaries $f^{\alpha}_{\min}$ and $f^{\alpha^m}_{\max}$ represent the far-left and far-right samples in $\{f^m_{\max(\mu)+r}\}$.
4) Exclude the sub-band frequencies $\{f^m_{\max(\mu)+r}\}$ from the set $\{f_\mu\}$: $\{f_{\mu>\delta}\} = \{f_{\mu>\delta}\} \setminus \{f^m_{\max(\mu)+r}\}$. If the resulting set is empty, the iteration can be stopped. If not, go back to 2) and increase the iteration counter m.

Once the iterative scheme above is finished in Step 4, a total of n_μ different interpolation models $\alpha^m(f)$ $(m = 1, \ldots, n_\mu)$ of the model uncertainty are identified. Each one of these interpolation models $\alpha^m(f)$ is only valid in a local frequency interval $f \in [f^{\alpha^m}_{\min}, f^{\alpha^m}_{\max}]$.

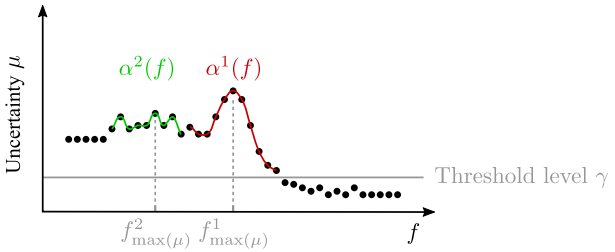

Fig. 3. Example uncertainty profile from which the interpolation models $\alpha^m(f)$ are derived. All samples below the threshold level γ are not considered in the creation of the interpolation models.

To provide a more comprehensive understanding of how the local interpolation algorithm operates, we can utilize an example scenario. Let us assume that we have an uncertainty profile, which can be visualized in Fig. 3. Initially, we exclude all samples for which the uncertainty level is below the specified threshold level, denoted by γ. Subsequently, we select the maximum value of the remaining samples, denoted by $f^1_{\max(\mu)}$, and use a total of $n_f = 5$ samples on either side of $f^1_{\max(\mu)}$ to construct the first cubic spline interpolation function, which can be represented as $\alpha^1(f)$. In the second iteration, the samples utilized in the interpolation of $\alpha^1(f)$ are excluded from the search space, and the maximum value is again identified, which correspond to $f^2_{\max(\mu)}$. Ideally, we would select a symmetric window around $f^2_{\max(\mu)}$; however, in this specific case, only three samples are available to the right of $f^2_{\max(\mu)}$, resulting in the use of an asymmetric window for the local interpolation function, represented as $\alpha^2(f)$. In the third and final iterations, only the left boundary region remains, where the uncertainty remains constant due to boundary effects. In this region, a random sample is selected to complete the local interpolation process.

Step 3 (Construction of the Sampling Metric): Now that local models for the uncertainty are available, they are used to steer the frequency sampling process. As the model uncertainty is a measure for undersampling, the most plausible sampling decision would be to let new frequency locations coincide with the maxima of different local interpolation models $\alpha^m(f)$. However, adoption of this sampling metric results in an AFS algorithm that does not function consistently. More specifically, the algorithm sometimes gets stuck in frequency regions where constantly new samples are added without lowering the uncertainty. The reason for this phenomenon is that taking decisions based on the local model uncertainty only, greatly favors exploitation but ignores exploration [30]. Exploitation generates new sampling frequencies based on information

obtained from previous sampling points, as is done with the local rational modeling. Exploration on the other hand performs this generation independently by, for example, taking a random sample.

To obtain a sampling metric that better balances exploitation and exploration, the uncertainty model is combined with the so-called crowding distance [31]. The crowding distance of a frequency point represents the density of frequency samples around that specific point. Given a certain local model $\alpha^m(f)$, the crowding distance $\mathrm{CD}^m(f)$ that is valid within the frequency range $[f_{\min}^{\alpha^m}, f_{\max}^{\alpha^m}]$ of that specific interpolation model is defined as follows:

$$\mathrm{CD}^m(f) = \sum_{r=-n_f}^{n_f} \left\| f - f^m_{\max(\mu)+r} \right\|_2^2 \quad \text{with } f \in \left[f_{\min}^{\alpha^m}, f_{\max}^{\alpha^m}\right]. \tag{10}$$

A large crowding distance reflects a small sampling density and vice versa. It is expected that in the frequency regions with larger crowding distances, relatively less information about the system is available. Incorporation of the crowding distance in the sampling metric, therefore, favors exploration independently of the model uncertainty. As the value of the crowding distance in (10) relies on the absolute difference between frequencies, it needs to be normalized to obtain a uniform metric across different frequency ranges. The normalized crowding distance is defined as follows [31]:

$$\mathrm{NCD}^m(f) = \frac{\max(\mathrm{CD}^m) - \mathrm{CD}^m(f)}{\max(\mathrm{CD}^m) - \min(\mathrm{CD}^m)}. \tag{11}$$

The eventual sampling metric β^m that combines the uncertainty α^m and the normalized crowding distance is constructed as follows:

$$\beta^m(f) = \alpha^m(f)\left(1 + \mathrm{NCD}^m(f)\right). \tag{12}$$

Step 4 (Addition of New Frequency Samples): The AFS algorithm bases itself on the sampling metric β^m to add new frequency samples. The frequency point $f^m_{\max}$ corresponding to the maximum of $\beta^m(f)$ is selected as the next frequency to be evaluated by the simulator. However, if $f^m_{\max}$ is too close to an already evaluated point (i.e., relative frequency difference smaller than 0.1%), the next location is randomly selected from $[f_{\min}^{\alpha^m}, f_{\max}^{\alpha^m}]$. The inclusion of this random selection increases the exploration capabilities of the AFS algorithm even further. Once new data samples of $\boldsymbol{X}(f^m_{\max})$ are obtained at different frequencies $f^m_{\max}$ for $m = 1, \ldots, n_\mu$; then, all $f^m_{\max}$ are added to the set $\{f_k\}$ and the adaptive sampling iteration is restarted from Step 1.

V. Numerical Examples

The proposed AFS algorithm is applied to several examples. First, an artificial example is generated on which we can demonstrate the basic functioning and performance of the algorithm. In the second example, a dual-band microstrip bandpass filter is analyzed. The final example examines an eight-port PCIe-2 module. A computer with an Intel i7-8665U CPU at 2.11 GHz has been used. All examples are compared with an established VF-based technique [7]. This technique relies on estimating multiple global rational models, each with a different model order. Subsequently, the two models that exhibit the highest accuracy are compared and a frequency sample is added to the region where these two models disagree the most. Antonini et al. [7] did not specify the maximal VF order that the model order selection needs to take into account given a certain number of samples. We choose to restrict the maximal VF order in each iteration to the number of samples minus the number of degrees of freedom used in the proposed local AFS technique. By doing so, we obtain a fair comparison between the two techniques in terms of the number of degrees of freedom.

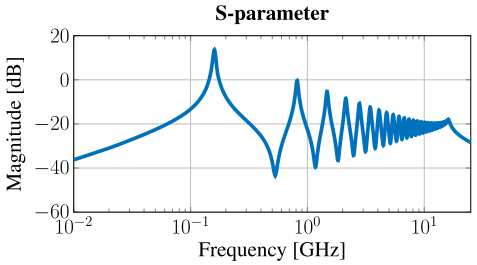

Fig. 4. Magnitude response and pole map of the artificial resonating system.

A. Artificial Resonating System

In the first example, an artificial system $H(s)$ has been generated that contains 25 complex pole pairs combined with a delay (see Fig. 4). The system's frequency-domain transfer function $H(s)$ is defined as follows:

$$H(s) = \sum_{i=1}^{25}\left(\frac{R_i}{s - p_i} + \frac{\overline{R_i}}{s - \overline{p_i}}\right)e^{-\tau s} \tag{13}$$

where s is the complex Laplace variable, and τ is the delay. R_i and p_i are, respectively, the complex residue and pole locations of the ith pole pair. $\overline{\bullet}$ is the complex conjugate operator. To achieve a magnitude response with a high dynamic range, the poles p_i are deliberately selected to ensure that the quality factor Q of each pole pair is equal to 25. This approach results in a pole pattern where each pole pair has a constant angle with the imaginary axis. Meanwhile, the residues R_i are randomly selected within the unit circle. We have furthermore added a time delay τ of 100 ps to the system ($\tau\, f_{\max} = 2.5$) that emulates the distributed behavior of a microwave system. Furthermore, we evaluate the performance of the proposed technique in two scenarios: one with $n_A = n_B = 4$ and another with $n_A = n_B = 6$. In both scenarios, the number of degrees of freedom q is chosen equal to 6. These choices correspondingly yield n_f values of 7 and 9, respectively. The accuracy threshold γ is set to 0.01 (−40 dB).

As the adaptive sampling algorithm progresses, more samples become available. Correspondingly, the uncertainty μ gives an increasingly better view of the regions, where new frequency samples are needed. Furthermore, more local sampling metrics $\beta^m(f)$ become available, which means that multiple samples can be added in parallel. This parallel addition is a major advantage of local modeling compared with global methods. In the $n_A = n_B = 4$ scenario, on average 34

iterations are needed in this example which results in an average total number of 179 samples to achieve an accuracy level below −40 dB over the frequency range of interest (0–25 GHz). Choosing $n_A = n_B = 6$, requires on average 29 iterations and an average total number of 128 samples to reach the same accuracy level. Remark that the total number of samples and iterations are no longer deterministic quantities. They partly depend on the locations of the random samples taken at the edges or when a new sample is relatively close to an existing one (see Section IV, Step 4).

To demonstrate the performance of the proposed AFS algorithm, the local approach is compared with the global VF-based AFS technique proposed in [7]. We selected the VF model for verification purposes because it is readily available and computationally convenient. However, other global modeling approaches can also be used. The VF-based approach involves 43 iterations, corresponding to a total of 54 samples. No stability constraints are applied to the pole locations during the estimation process. In Fig. 5, we compare the relative error of the local LRM-based approach, with $n_A = n_B = 4$, and $n_A = n_B = 6$, to the VF-based approach. The local LRM-based approach consistently exhibits a relative error below −40 dB across the entire frequency spectrum. While the global VF-based approach demonstrates excellent performance at lower frequencies, it experiences an increased relative error in the frequency range from 10 to 15 GHz. This discrepancy arises from the VF-based approach's inadequacy in selecting sufficient samples within this frequency region to distinguish additional dynamic behavior. This limitation arises from the global approach's termination decision, which relies on the discrepancies between the two best VF models in a given iteration. Consequently, the VF-based approach may not adequately capture all the system dynamics in the specified frequency range. The local LRM-based approach mitigates this limitation by using an uncertainty metric that compares the model against the original data, without necessitating comparisons among multiple models.

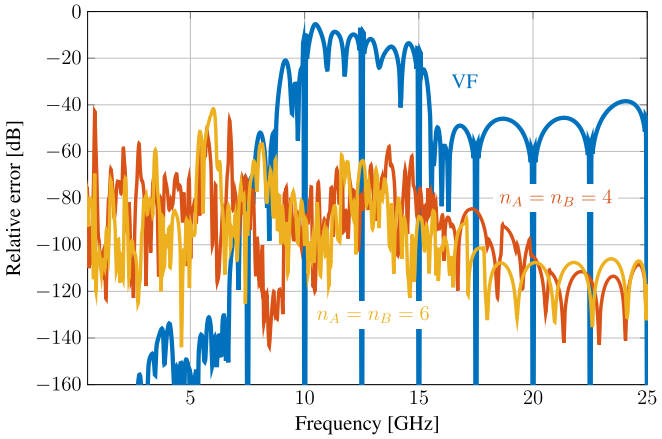

Fig. 5. Comparison between the relative error of the local LRM-based approach and the global VF-based approach.

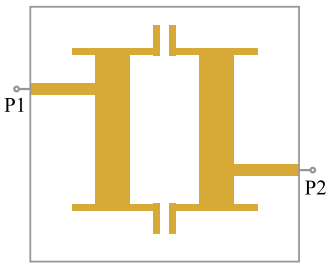

Fig. 6. Top view of the dual-band microstrip bandpass filter used in example B. P1 and P2 represent the ports of the structure.

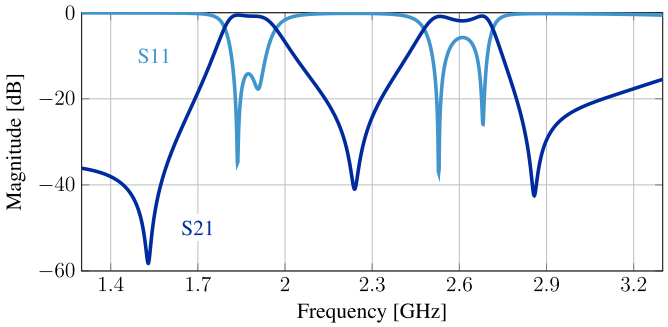

Fig. 7. Simulated S_{11} and S_{21} of the dual-band bandpass filter.

B. Dual-Band Microstrip Bandpass Filter

In the second example, a dual-band microstrip bandpass filter is analyzed (see Fig. 6) [32]. A Rogers RO4003 substrate is used with a relative dielectric constant of 3.55, a dielectric height of 1.542 mm, and a loss tangent of 0.0022. The EM behavior of the filter is simulated using the Advanced Design System (ADS) software suite. The frequency region of interest is between 1.3 and 3.3 GHz. The simulated S-parameters clearly show two passbands that are closely spaced (see Fig. 7). We choose $n_A = n_B = 6$ and $q = 6$ in this example, which correspond to an n_f equal to 8. The accuracy threshold γ equals 0.01 (−40 dB).

The adaptive sampling algorithm requires on average of six iterations with an average total number of 39 samples. A comparison with the VF-AFS proposed in [7] is also performed (Fig. 8). The VF-based algorithm chooses 27 samples (19 iterations) over the frequency range of interest and targets the same relative error accuracy as the proposed LRM-based approach. Through model order selection the VF-based algorithm determined that 21 poles are optimal to reach the accuracy requirements. As further validation, we compare the accuracy of the LRM and VF models generated by the proposed LRM-based and the VF-based algorithms over a dense grid of 1001 frequency samples (8). The plots in Fig. 8 show that the LRM-based approach reaches an average relative error below −80 dB, while the VF-based algorithm reaches a consistent relative error below −50 dB.

In each iteration of the proposed AFS algorithm, two CPU time components are present: one (EM solver dependent) related to EM calculations at a set of frequency samples and another one (EM solver independent) related to all the rest (local model generation and metrics computations). We focus on the second component in what follows to show the computational efficiency of the proposed algorithm. For this two-port system, the generation time for one local rational model is

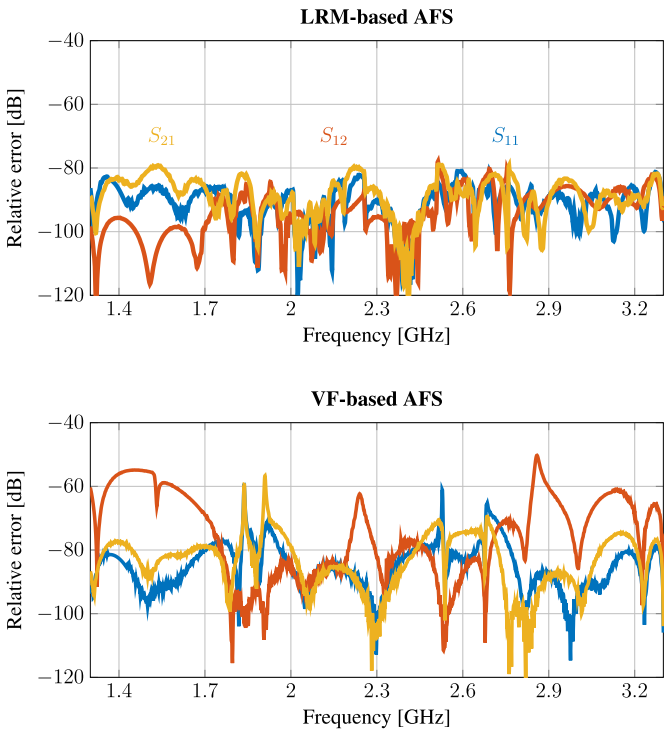

Fig. 8. Bandpass filter comparison of the relative error of the LRM-based approach with the VF-based approach of [7].

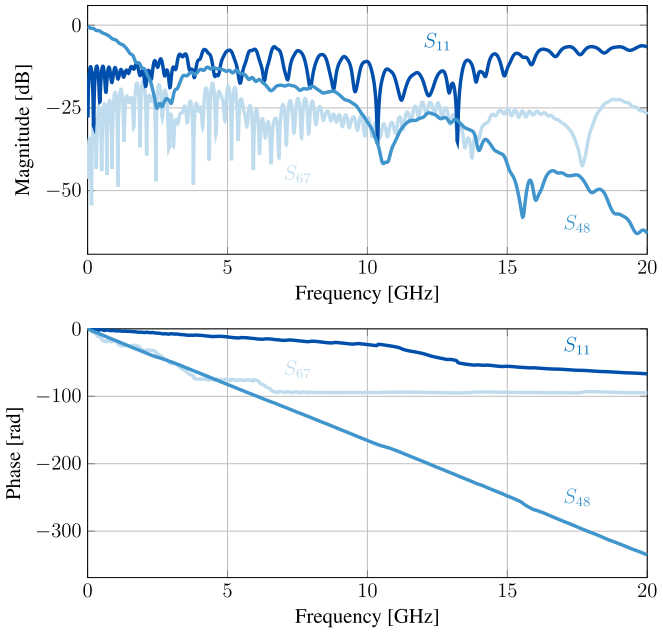

Fig. 9. Amplitude and phase response of three arbitrarily selected S-parameters of the PCIe-2 module. A total of 64 S-parameters are available.

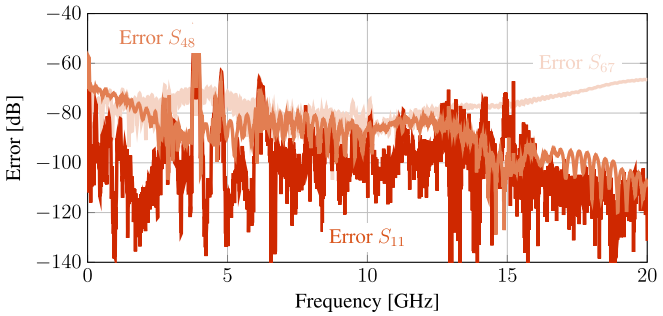

Fig. 10. Comparison of modeling prediction errors obtained using local rational models as a function of frequency for the PCIe-2 example.

on average 4 ms. The number of local rational models that need to be estimated depends on the number of frequency samples that are added in a certain iteration. As a result, the total computation time varies with the iteration count. The maximum recorded computation time to complete one iteration is 150 ms. On average of six iterations are needed. Therefore, the EM solver independent CPU time component of the proposed AFS algorithm results to be very efficient. Note that the cumulative estimation time for the VF models in the VF-based approach amounts to 1.76 s, while the LRM-based approach needs 0.9 s.

C. PCIe-2 Module

As a final example, we consider a channel simulation of a Peripheral Component Interconnect Express (PCIe) Gen 2.0 module. This example is part of the signal integrity design kit in ADS and is considered as one of the reference examples for signal integrity applications. The simulated PCIe module comprises four multiconductor transmission lines that establish connections between a four-port transmitter and a four-port receiver. Consequently, the module consists of a total of eight ports, resulting in a 8×8 S-parameter matrix. It is important to note that due to the long electrical length of the transmission lines, multiple differing delays are present in the simulated phase profiles. The frequency range of interest is between 0 and 20 GHz. Due to the complexity of the dynamic variations, we choose $n_A = n_B = 8$ and $q = 6$ in this example. This choice translates into a sub-band width of 19 samples. The accuracy threshold γ is again set to 0.01 (-40 dB). Fig. 9 shows the amplitude and phase responses of three arbitrarily selected S-parameters of the PCIe-2 module.)

On average, the adaptive sampling algorithm requires 98 iterations, with a total of 1310 samples. The average estimation time for one local rational model is 87 ms. Unlike previous examples, it is not possible to assess the adaptive sampling quality using a global VF model in this case. The model order for a global VF model has been gradually increased up to order 1000, but none of these global models achieve an acceptable relative accuracy level below -10 dB across the entire frequency range. This is due to significant distributed effects (delays) in this example. Therefore, the global VF model cannot be used for showing results related to the adaptive sampling quality as in the previous examples. Furthermore, a comparison with the VF-based algorithm [7] is attempted, but proved very difficult within a reasonable timeframe due to the notable distributed effects, particularly delays, present in this example. To reach 750 samples with the VF-based algorithm, it took more than one day of estimation time. While the accuracy of the standard VF model can be improved by employing multidelay rational modeling techniques [33], [34], this topic is beyond the scope of this article. However, irrespective of a global model, we can evaluate the model prediction

quality of the local rational models across the entire frequency range. For this purpose, the local rational models are evaluated at multiple frequency samples different from those used during estimation in the AFS process. Fig. 10 illustrates the absolute error profiles for the S-parameters S_{11}, S_{48}, and S_{67}. The error profiles demonstrate the consistent performance of the local rational models across the frequency range, maintaining an error level below -55 dB. This indicates that, besides guiding the adaptive sampling algorithm, the local rational models can also serve as an accurate frequency-domain macromodeling tool.

VI. Conclusion

We have introduced a new AFS algorithm using local rational modeling. This approach offers several advantages over AFS techniques relying on global models. First, our algorithm eliminates the need for model order selection during its execution. In addition, it is better equipped to handle the distributed behavior commonly found in microwave systems. To validate the effectiveness of our method, we conducted numerous numerical examples, which consistently demonstrated its accuracy and efficiency. The algorithm successfully identifies the most informative samples of the frequency-domain response of microwave systems while maintaining an effective exploration capability.

References

[1] R. F. Harrington, *Field Computation by Moment Methods*. New York, NY, USA: Macmillan, 1968.

[2] J. Jin, *The Finite Element Method in Electromagnetics*, 3rd ed. Hoboken, NJ, USA: Wiley, Mar. 2014.

[3] A. E. Ruehli, G. Antonini, and L. Jiang, *Circuit Oriented Electromagnetic Modeling Using the PEEC Techniques*. Hoboken, NJ, USA: Wiley, 2017.

[4] L. Lombardi, D. Romano, and G. Antonini, "Efficient numerical computation of full-wave partial elements modeling magnetic materials in the PEEC method," *IEEE Trans. Microw. Theory Techn.*, vol. 68, no. 3, pp. 915–925, Mar. 2020.

[5] T. Dhaene, J. Ureel, N. Fache, and D. De Zutter, "Adaptive frequency sampling algorithm for fast and accurate S-parameter modeling of general planar structures," in *IEEE MTT-S Int. Microw. Symp. Dig.*, Sep. 1995, pp. 1427–1430.

[6] Y. Ding, K.-L. Wu, and D. Gang Fang, "A broad-band adaptive-frequency-sampling approach for microwave-circuit EM simulation exploiting Stoer-Bulirsch algorithm," *IEEE Trans. Microw. Theory Techn.*, vol. 51, no. 3, pp. 928–934, Mar. 2003.

[7] G. Antonini, D. Deschrijver, and T. Dhaene, "Broadband rational macromodeling based on the adaptive frequency sampling algorithm and the partial element equivalent circuit method," *IEEE Trans. Electromagn. Compat.*, vol. 50, no. 1, pp. 128–137, Feb. 2008.

[8] G. Antonini, D. Deschrijver, and T. Dhaene, "Efficient power-bus modeling based on an adaptive frequency sampling technique," *Int. J. Numer. Model., Electron. Netw., Devices Fields*, vol. 22, no. 1, pp. 57–76, Jan. 2009.

[9] P. Li, Y. Li, L. J. Jiang, and J. Hu, "A wide-band equivalent source reconstruction method exploiting the Stoer-Bulirsch algorithm with the adaptive frequency sampling," *IEEE Trans. Antennas Propag.*, vol. 61, no. 10, pp. 5338–5343, Oct. 2013.

[10] S. De Ridder, D. Deschrijver, D. Spina, T. Dhaene, and D. V. Ginste, "A Bayesian approach to adaptive frequency sampling," in *Proc. IEEE 23rd Workshop Signal Power Integrity (SPI)*, Jun. 2019, pp. 1–4.

[11] G. J. Burke, E. K. Miller, S. Chakrabarti, and K. Demarest, "Using model-based parameter estimation to increase the efficiency of computing electromagnetic transfer functions," *IEEE Trans. Magn.*, vol. 25, no. 4, pp. 2807–2809, Jul. 1989.

[12] B. Gustavsen and A. Semlyen, "Rational approximation of frequency domain responses by vector fitting," *IEEE Trans. Power Del.*, vol. 14, no. 3, pp. 1052–1061, Jul. 1999.

[13] B. Gustavsen, "Improving the pole relocating properties of vector fitting," *IEEE Trans. Power Del.*, vol. 21, no. 3, pp. 1587–1592, Jul. 2006.

[14] V. de la Rubia and Z. Peng, "Data-driven model order reduction via Loewner approach for fast frequency sweep in hybrid BI-FEM solution in large finite frequency selective surfaces," in *IEEE MTT-S Int. Microw. Symp. Dig.*, May 2017, pp. 287–289.

[15] S. Grivet-Talocia and B. Gustavsen, *Passive Macromodeling* (Wiley Series in Microwave and Optical Engineering). Hoboken, NJ, USA: Wiley, Nov. 2015.

[16] R. Pintelon and J. Schoukens, *System Identification: A Frequency Domain Approach*. Hoboken, NJ, USA: Wiley, 2012.

[17] D. Peumans, R. Pintelon, J. Lataire, and G. Vandersteen, "Frequency response function measurements of multivariable systems via local rational modeling," *IEEE Trans. Instrum. Meas.*, vol. 70, pp. 1–9, 2021.

[18] D. Deschrijver and T. Dhaene, "Adaptive knot placement for rational spline interpolation of sparse EM-based data," in *Proc. 17th Int. Conf. Appl. Electromagn. Commun. (ICECom)*, Oct. 2003, pp. 433–436.

[19] D. Deschrijver, B. Gustavsen, and T. Dhaene, "Fast broadband modeling of frequency-domain responses by piecewise interpolation," *Electr. Power Syst. Res.*, vol. 79, no. 11, pp. 1574–1578, Nov. 2009.

[20] F. Ferranti, L. Knockaert, and T. Dhaene, "Passivity-preserving parametric macromodeling by means of scaled and shifted state-space systems," *IEEE Trans. Microw. Theory Techn.*, vol. 59, no. 10, pp. 2394–2403, Oct. 2011.

[21] E. Van Nechel, F. Ferranti, Y. Rolain, and J. Lataire, "Model-driven design of microwave filters based on scalable circuit models," *IEEE Trans. Microw. Theory Techn.*, vol. 66, no. 10, pp. 4390–4396, Oct. 2018.

[22] W. Zhang, F. Feng, J. Zhang, Z. Zhao, J. Ma, and Q.-J. Zhang, "Parallel decomposition approach to wide-range parametric modeling with applications to microwave filters," *IEEE Trans. Microw. Theory Techn.*, vol. 68, no. 12, pp. 5288–5306, Dec. 2020.

[23] F. Feng, W. Na, J. Jin, W. Zhang, and Q.-J. Zhang, "ANNs for fast parameterized EM modeling: The state of the art in machine learning for design automation of passive microwave structures," *IEEE Microw. Mag.*, vol. 22, no. 10, pp. 37–50, Oct. 2021.

[24] R. Pintelon, J. Schoukens, G. Vandersteen, and K. Barbé, "Estimation of nonparametric noise and FRF models for multivariable systems—Part I: Theory," *Mech. Syst. Signal Process.*, vol. 24, no. 3, pp. 573–595, Apr. 2010.

[25] H. Van hamme and R. Pintelon, *Application of the Bootstrapped Total Least Squares (BTLS) Estimator in Linear System Identification* (Signal Processing VI: Theories and Applications), vol. 2, J. Vandewalle, R. Boite, M. Moonen, and A. Oosterlinck, Eds. Amsterdam, The Netherlands: Elsevier, Aug. 1992, pp. 731–734.

[26] U. Beyer and F. Śmieja, "Data exploration with reflective adaptive models," *Comput. Statist. Data Anal.*, vol. 22, no. 2, pp. 193–211, Jul. 1996.

[27] P. J. Davis, *Interpolation Approximation*. Chelmsford, MA, USA: Courier Corporation, 1975.

[28] C. A. Hall and W. W. Meyer, "Optimal error bounds for cubic spline interpolation," *J. Approximation Theory*, vol. 16, no. 2, pp. 105–122, Feb. 1976.

[29] Z. Zhang and C. F. Martin, "Convergence and Gibbs' phenomenon in cubic spline interpolation of discontinuous functions," *J. Comput. Appl. Math.*, vol. 87, no. 2, pp. 359–371, Dec. 1997.

[30] J. Chen, B. Xin, Z. Peng, L. Dou, and J. Zhang, "Optimal contraction theorem for exploration–exploitation tradeoff in search and optimization," *IEEE Trans. Syst., Man, Cybern. A, Syst. Humans*, vol. 39, no. 3, pp. 680–691, May 2009.

[31] J. Zhang, S. Chowdhury, and A. Messac, "An adaptive hybrid surrogate model," *Struct. Multidisciplinary Optim.*, vol. 46, no. 2, pp. 223–238, Aug. 2012.

[32] C.-Y. Hsu, C.-Y. Chen, and H.-R. Chuang, "Microstrip dual-band bandpass filter design with closely specified passbands," *IEEE Trans. Microw. Theory Techn.*, vol. 61, no. 1, pp. 98–106, Jan. 2013.

[33] M. Zyari and Y. Rolain, "Identifying multiple reflections in distributed-lumped high-frequency structures," *IEEE Trans. Microw. Theory Techn.*, vol. 64, no. 4, pp. 1306–1312, Apr. 2016.

[34] M. Z. Y. Rolain, F. Ferranti, G. Vandersteen, and P. Bronders, "Multi-delay rational modeling of lumped-distributed systems," in *IEEE MTT-S Int. Microw. Symp. Dig.*, Jun. 2017, pp. 1624–1627.

Dries Peumans (Member, IEEE) was born in Brussels, Belgium, in 1992. He received the M.Sc. and Ph.D. degrees in electrical engineering (electronics and information technology) from Vrije Universiteit Brussel (VUB), Brussels, in 2015 and 2020, respectively.

He is currently an Assistant Professor with the Department of Fundamental Electricity and Instrumentation (ELEC), VUB. His research interests include broadband RF characterization, data-driven modeling techniques, and behavioral modeling of complex microwave circuits.

Sander De Keersmaeker (Student Member, IEEE) was born in Brussels, Belgium, in 1996. He received the M.Sc. degree in physics from Vrije Universiteit Brussel (VUB), Brussels, in 2020.

Since October 2020, he has been a Ph.D. Researcher with the Department of ELEC, VUB. His research interests include signal-dependent behavioral modeling of RF devices.

Cedric Busschots (Member, IEEE) was born in Leuven, Belgium, in 1990. He received the M.Sc. degree in industrial engineering (electronics-ICT) from Lessius Mechelen, Campus De Nayer, Antwerp, Belgium, in 2012, the M.Sc. degree in electromechanical engineering from Vrije Universiteit Brussel (VUB), Brussels, Belgium, in 2015, and the Ph.D. degree in electrical engineering from VUB in 2022.

He is currently a Researcher with the Royal Belgian Institute for Space Aeronomy, Brussels.

Yves Rolain (Fellow, IEEE) was born in Belgium, in 1961. He received the dual M.Sc. degree in electrical engineering (Burgerlijk Ingenieur) and computer sciences, and the Ph.D. degree in applied sciences from Vrije Universiteit Brussel (VUB), Brussels, Belgium, in 1984, 1986, and 1993, respectively.

He is currently a Professor with the Department of ELEC, VUB. His current research interests are microwave measurements and modeling, applied digital signal processing, and system identification.

Dr. Rolain received the IEEE Instrumentation and Measurement Society Award in 2005.

Francesco Ferranti (Senior Member, IEEE) received the Ph.D. degree in electrical engineering from Ghent University, Ghent, Belgium, in 2011.

He is currently a Professor with the Department of Applied Physics and Photonics, Brussels Photonics, Vrije Universiteit Brussel, Brussels, Belgium. He is also an Adjunct Professor with the Indian Institute of Technology (IIT) Madras, Chennai, India, and an Adjunct Professor with Carleton University, Ottawa, ON, Canada. His research interests include data-driven and model-driven modeling techniques, sampling techniques, design space exploration, uncertainty quantification, optimization, microwave, photonics, applied electromagnetics, and behavioral modeling.

Dr. Ferranti is a member of the Technical Committee on Design Automation (MTT-2) of the IEEE Microwave Theory and Techniques (MTT) Society. He was a recipient of the Anile-ECMI Prize for Mathematics in Industry 2012 and the Electromagnetic Compatibility Society President's Memorial Award in 2012. He serves as a regular reviewer for several international journals and conferences. He is currently an Associate Editor for IEEE TRANSACTIONS ON MICROWAVE THEORY AND TECHNIQUES.